Chapter 9
Skutterudites: Progress and Challenges

Gerda Rogl and Peter Rogl

Abstract Since the discovery of skutterudite (an arsenide mineral (Co, Fe, Ni)As_3) in 1845 in Norway, valuable research on isotypic Sb-based skutterudites achieved high-quality thermoelectric (TE) *p*- and *n*-type leg materials with remarkably high figure-of-merit ZT, forming the basis for large-scale production and application in thermoelectric power generation coupled with waste heat recovery.

We will cover the most important steps within these almost 200 years and discuss the development of TE skutterudites and the enhancement of those figures-of-merit. Besides unfilled $CoSb_3$-based grades, we will focus on filled *p*- and *n*-type skutterudites ($La_{1-x}Fe_4Sb_{12}$), to show improvement via tuning of the electronic band structure, to consider phonon engineering in order to reduce thermal conductivity, to discuss the nanoeffect (ball milling, high-energy ball milling, severe plastic deformation), and to highlight the importance of density and impact of nanoprecipitates. Issues concerning the stability of skutterudites and an overview of mechanical properties including thermal expansion will follow. Although laboratory records in the figure-of-merit ZT equal to 1.5 for *p*-type and 1.9 for *n*-type skutterudites were reached, large-scale production (about 50 kg batches of powders) has already achieved ZT values of 1.3 (*p*-type) and 1.5 (*n*-type) with thermoelectric conversion leg efficiencies of 13.4 and 14.5%. With these attractive values, one can conceive TE skutterudite materials being at the brink of a breakthrough in technological applications for thermoelectric power generation, given a large-scale thermoelectric (TE)-generator module producer.

9.1 Introduction

Thermoelectric (TE) materials, i.e., *n*- and *p*-type heavily doped semiconductors, have the ability to convert a heat flow from an external source (thermal radiation energy flow) into a flow of charge carriers within the material (i.e., electric current

G. Rogl (✉) · P. Rogl
Christian Doppler Laboratory for Thermoelectricity, Institute of Materials Chemistry, University of Vienna, Wien, Austria

Institute of Solid State Physics, TU Wien, Wien, Austria
e-mail: gerda.rogl@univie.ac.at

S. Skipidarov, M. Nikitin (eds.), *Novel Thermoelectric Materials and Device Design Concepts*, https://doi.org/10.1007/978-3-030-12057-3_9

and, hence, electric power). Many classes of materials like tellurides, silicides, copper selenides, oxides, zinc tellurides, antimonides, Zintl phases, clathrates, half-Heusler alloys, or skutterudites qualify as TE materials.

The most important features in favor to use skutterudites as TE materials are as follows:

1. Starting and raw materials are abundant and cheap in comparison to other TE materials.
2. Wide temperature range of operation (from room temperature to 900 K).
3. High TE quality.
4. Long-term stability of thermoelectric performance.
5. Reasonably good mechanical properties.

The quality of TE material depends usually on two properties. The first one is the figure-of-merit, $ZT = S^2\sigma T/\kappa$, where S, σ, and κ are Seebeck coefficient, electrical conductivity, and thermal conductivity, respectively, κ consisting of electron κ_{el} and lattice κ_L parts. Therefore, a good TE material should have a large absolute value $|S|$, high σ, but low κ. The second property is the conversion efficiency η (for electric power generation):

$$\eta = \frac{T_h - T_c}{T_h} \times \frac{\sqrt{1 + ZT_{avg}} - 1}{\sqrt{1 + ZT_{avg}} + \frac{T_c}{T_h}}, \tag{9.1}$$

where T_h and T_c are temperatures on hot and cold side and ZT_{avg} is the average ZT value in the temperature gradient between T_c and T_h. ZT_{avg} has to be evaluated integrating all measured data, as the curvature of ZT vs. T curve determines the result. Kim et al. [1] use a similar approach with detailed calculation, resulting in ZT_{eng} instead.

In various review articles [2–13], TE materials and/or skutterudites have been widely discussed. In this review we want to guide the reader through the development of skutterudites and those high ZT and efficiencies. We will show how easily skutterudites can be produced in the laboratory, as well as, in large quantities, discuss the problem of long-term stability and production of TE modules and generators. All that will be done step by step.

9.2 A Short Review of the History of Skutterudite Thermoelectrics

In 1828 Oftedal [14] identified the crystal structure of a new mineral, MAs_3 (M = Co or Ni), which was found in Norway near the small town of Skutterud. He identified the crystal structure as body-centered cubic, containing 32 atoms per unit cell, belonging to the space group *Im*-3 No. 204. The general formula of binary skutterudites is MX_3 where M is a transition metal and X a pnictogen atom (P, As, Sb). The unit

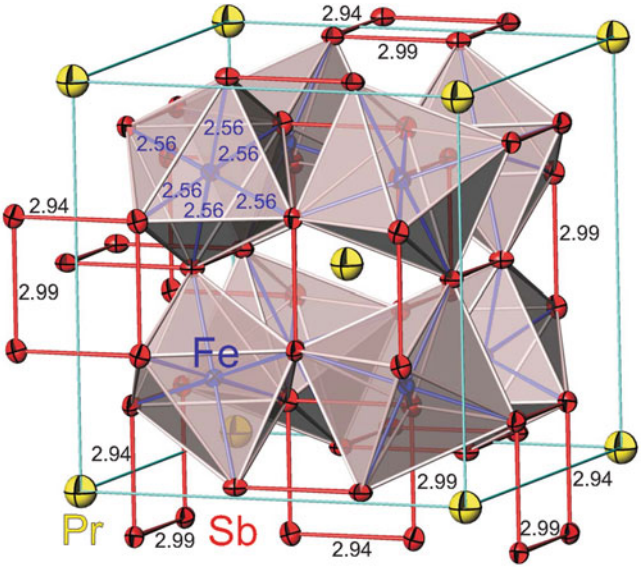

Fig. 9.1 Unit cell (in light blue) of filled skutterudite $PrFeSb_{12}$, highlighting Fe-centered, tilted Sb octahedra and red Sb rectangles. Numbers are interatomic distances in Å

cell is built of eight tilted but corner-connected octahedra formed by pnictogen atoms (Fig. 9.1). The transition metal atoms occupy 8*c* sites (¼, ¼, ¼) at octahedral centers. Six of the eight sub-cubes of the unit cell are filled with planar rings of pnictogens, occupying 24*g* sites (0, *y*, *z*). Two icosahedral voids at 2*a* sites ((0, 0, 0) and (½, ½, ½)) can be stuffed with filler atoms, which should have ionic radii smaller than the cage volume in order to be loosely bound developing so-called rattling vibrations (for further details see below). In the 1970s Kjekshus et al. [15] showed that pnictogen atoms in skutterudites do not fulfill Oftedal relation for 24*g* sites: $2(y + z) = 1$. Therefore, he replaced the square pnictogen rings by rectangular ones.

In parallel to structure studies, already in the early 1950s of the twentieth century, Dudkin and Abrikosov [16] found that $CoSb_3$ had high electrical resistivity ρ combined with very high thermal conductivity κ. In addition, they studied the influence of Ni as dopant on ρ and hardness, both properties decreasing with increasing in Ni content. Also, other groups investigated the influence of dopants (Ni, Fe, Cu, Al, Ti, Zr), but all these attempts failed to produce useful TE materials because even though Fe and Ni could reduce κ, it still remained very high. Because of this high κ, ZT of $CoSb_3$ remained below 0.2 in the following years [17–19]. Furthermore, TE properties were found to change drastically dependent on the preparation method, and even a change from *p*- to *n*-type can occur as a function of temperature. Consequently, a breakthrough for $CoSb_3$ was not possible so far.

However, a first breakthrough in the development of skutterudites as TE materials arose with the appearance of filled skutterudites $E_yM_4X_{12}$ in 1977 [20], where E can be any electropositive element (lanthanoid, actinoid, alkaline, or alkaline earth) partially or fully occupying the voids in 2a sites. Fig. 9.1 reveals details on interatomic distances in $PrFeSb_{12}$. It should be mentioned that the transition metal atom exhibits uniform bonds to the vertices of non-regular Sb octahedra.

Concerning the ideal fillers, theory and experiment differ. Theoretically, optimal void fillers would be neutral atoms (e.g., Xe) with large atomic displacement parameters that would ensure enhanced scattering of heat-carrying phonons, thereby inferring a large reduction in the lattice thermal conductivity κ_L but only a minimum perturbation of electron transport properties. However, in praxis, so far, it was not possible to keep such rare gas species locked in the skutterudite cage [3].

Various review papers, e.g., Uher [3] and Rull-Bravo et al. [6], provide a detailed overview of the development of filled skutterudites; therefore, here only some benchmarks will be discussed.

In 1994 Slack and his group [21, 22] proposed the "phonon-glass electron-crystal" (PGEC) concept for a compound thermally conducting like a glass (low κ, low mobility, low effective mass) and at the same time conducting charge like an electron-crystal (high charge mobility, high S and high σ). For good TE materials, such a combination can indeed be found in filled skutterudites, as the rattling motion of the fillers interferes with the normal modes of the structure, reducing κ_L. Due to weak coupling of the filler with the rest of the structure and the fact that pnictogen orbitals are hardly affected by the rattling ions, the mobility of charge carriers remains large, and, therefore, the structure can keep its crystalline character and good electronic properties. The smaller and heavier the ion in the void is, the higher is atom disorder, and the lower is the phonon part of the thermal conductivity. This "PGEC model" can be regarded as a benchmark in the development of filled skutterudites as TE materials.

At about the same time, in year 1993, Hicks and Dresselhaus [23] showed theoretically that by using two-, one-, or even zero-dimensional structures, it is possible to decouple TE parameters, S, σ, and κ. Venkatasubramanian [24] and Chen [25] later backed up these ideas, showing that a significant reduction in κ_L is possible via nanostructuring, so a new approach to get higher ZT values was born.

In the 1990s and at the beginning of the twenty-first century, researchers all over the world experimented with various fillers for single, double, and multi-filled skutterudites, as well as with Fe/Co, Fe/Ni, and Co/Ni substitution and even doping at Sb site (see Sect. 9.5.1, band structure engineering) and in parallel with nanostructuring and nanocomposites (see Sect. 9.5.2, phonon engineering), in order to obtain TE materials with highly optimized TE power factors and ZT.

9.3 Why Do We Focus on Sb-Based Skutterudites?

Generally, for unfilled MX_3 or filled $E_yM_4X_{12}$ skutterudites, all elements of the fourth, fifth, and sixth main groups of the periodic table would qualify for X; however, skutterudites cannot be formed with most of these elements, whereas for $X = P$, As, Sb, it works well. As- and P-based skutterudites have been investigated but in most cases not for thermoelectric purposes. With As being toxic and P forming rather small cages suppressing rattling modes, these elements do not qualify for TE applications. Sb-based skutterudites have been studied most, as attractive ZT values could be reached due to high mobility of charge carriers, high atomic masses, high σ, and large S.

9.4 Preparation Methods on Lab Scale

In order to study physical and mechanical properties of any material, sufficiently large and homogeneous samples are a prerequisite. Although single crystals might have various advantages, these crystals are not necessary as skutterudites have a cubic structure and anisotropy is not a main concern.

A huge variety of preparation methods have been proposed for filled skutterudites, such as high-pressure-high-temperature synthesis, high-pressure synthesis, high-pressure torsion, induction melting, pulse plasma sintering, self-propagation synthesis, gas atomization, chemical synthesis routes, and melt-spinning followed by spark plasma sintering (for details see Ref. [10] and refs. therein). Although some of these methods were propagated as "fast" or even "super rapid," in most cases, results were rather poor, e.g., ZT = 0.9 (~670 K) for $Yb_yCo_4Sb_{12}$ and ZT < 0.2 (~580 K) for $Mm_{0.3}Fe_3CoSb_{12}$, where mischmetal, Mm, is a multifiller (consisting of 50.8% Ce + 28.1% La + 16.1% Nd + 5% Pr), both melt-spun and spark plasma sintered [26], ZT = 0.6 at 673 K for $In_{0.5}Co_4Sb_{11.5}Te_{0.5}$ with high-pressure-high-temperature synthesis [27] or ZT = 1 at 760 K for $Nd_{0.9}Fe_3CoSb_{12}$ via induction melting [28].

The most successful method to produce homogeneous polycrystalline dense specimens is still based on the preparation method already used by Dudkin in the late 1950s [16] (melting-annealing method). A master alloy is prepared in an evacuated and sealed quartz ampoule from Co(Fe,Ni) and Sb by melting and quenching on air. The appropriate amount of fillers is added to this bulk, again sealed in a quartz ampoule under vacuum, annealed for a couple of hours after which the temperature is slowly increased to the melting temperature. It turned out that additional annealing is not necessary. Therefore, after melting (still inside the quartz ampoule), the sample can be quenched on air and then crushed into small pieces prior to ball milling or high-energy ball milling followed by hot pressing or spark plasma sintering for densification. If well performed, this melting-annealing technique takes not more time than 48 h including ball milling and hot pressing

[29]. Various groups use the basics of this route; however, it is, of course, necessary to optimize ball milling and hot pressing conditions [30] in order to get dense samples with fine grains, as these properties influence severely the TE performance [31].

Sesselmann et al. [32] compared TE properties of $Ce_{0.6}Fe_2Co_2Sb_{12}$ (nominal composition) from various synthesis routes: (1) gas atomization, (2) conventional melting-annealing method, and (3) antimony master alloys $Fe_xCo_{1-x}Sb_2$ and $CeSb_2$ by ball milling and hot pressing. It turned out that these three methods lead to different final compositions of the skutterudite phase and secondary phases, which influence significantly all TE properties of the material. For method (3) the highest ZT = 0.7 at 700 K was reached.

9.5 Enhancement of ZT for *p*- and *n*-Type Skutterudites

9.5.1 Band Structure Engineering

Fillers

In the late 1990s, as soon as researchers had found out that filling the icosahedral voids in the crystal structure of the skutterudite with so-called rattlers increases in the number of phonon scattering centers and this way indeed reduces κ_L, the search for the best filler (single-filled skutterudites) or fillers (double- and multi-filled skutterudites) had started.

Slack and Tsoukala [21], e.g., investigated unfilled $IrSb_3$ and predicted that inserting impurities into the lattice voids could reduce κ and lead to better TE properties. Anisotropic interactions arising from the nonmetal (X) sublattice were already suggested by Kjekshus et al. [15] as the principal source of the deviation from Oftedal relation, i.e., a rectangular distortion of X_4 groups. Although a series of skutterudites may follow Oftedal relation, the bulk of skutterudites and, particularly, thermoelectric, filled skutterudites reveal a rectangular deviation from square X_4 groups. Large atom thermal displacement parameters, as derived from X-ray/neutron diffraction data for filler atoms, are consistent with low-frequency vibrational modes (Einstein oscillations) seen in heat capacity measurements with energies around 6 meV (~70 K) and 18 meV (200 K). Ab initio, lattice dynamics calculations [33] suggest that filler atom and Sb vibrations are coherently coupled in good agreement with experimental evidence from high-resolution inelastic neutron scattering data [34, 35]. It was concluded that the strong reduction in thermal conductivity results from the interaction between the vibrational dynamics of electropositive filler atoms with the acoustic phonons of M_4Sb_{12} matrix [36].

The mostly used fillers are alkaline (Li, Na, K, Rb), alkaline earth (Ca, Sr, Ba), and rare earth (La, Ce, Pr, Nd, Sm, Eu, Yb) elements, but also In [37–40], Sn [41–44], Ti [45, 46], and I [47, 48] have been tried successfully. In the beginning it was assumed that all voids are fully occupied; however, Chen et al. [49]

compared the amount of Ce in $Ce_yFe_4Sb_{12}$ and $Ce_yFe_{4-x}Co_xSb_{12}$, and they found that y decreases with increasing Co content and that for pure Co_4Sb_{12}, only 10% of the voids can be filled. Still, it could be shown that already a small amount of filling fraction can reduce thermal conductivity significantly [4, 22, 34, 50].

Calculating the limit of filling level and optimal filling fraction [51–53], one can tune TE properties of filled skutterudites via the adjustable filling fraction. Theoretical and experimental filling fraction limits were summarized by Shi et al. [51, 54]. Furthermore, for thermodynamic stability of filled skutterudites, the electronegativity of the filler minus the electronegativity of Sb must be bigger than 0.8 [55]. Yang et al. [56] showed theoretically that the more the resonance frequencies of two guest atoms differ from each other, the higher is the phonon scattering efficiency. These findings were the kickoff for experimentalists to produce double-, triple- and multi-filled skutterudites keeping always in mind that the fillers should have different ionic radii, masses, and atom vibration frequencies.

Lu et al. [57] were the first to introduce two fillers, and with $Ce_{0.1}La_{0.2}FeCo_3Sb_{12}$, ZT = 0.6 was reached at 773 K. For a long time, triple-filled $Ba_{0.08}La_{0.05}Yb_{0.04}Co_4Sb_{12}$ had the highest ZT = 1.7 at 850 K [54] till this value could be topped by ZT = 1.8 at 800 K for $Sr_{0.07}Ba_{0.07}Yb_{0.07}Co_4Sb_{12}$ before and ZT = 1.9 at 835 K after high-pressure torsion processing.

The natural double filler didymium, DD (consisting of 4.76% Pr and 95.24% Nd), and the multifiller, mischmetal, Mm, (consisting of 50.8% Ce + 28.1% La + 16.1% Nd + 5% Pr) have proven to be ideal fillers for p-type skutterudites, reaching ZT higher than 1.2 [58–62].

Substitutions

As already shown at the example of $CoSb_3$ [16], another route to enhance TE properties is by substitution at Co site, usually by similar elements with a higher number of electrons, which act as donors and thereby increase σ. For n-type skutterudites Ni, but also Pd and Pt are used to substitute for Co [63, 64]. Expensive Pt and Pd showed good results, but do not qualify for mass production. Substituting Ni for Co increases σ and thermopower because each Ni atom acts as electron donor. Dudkin and Abrikosov [16], however, found that if the Ni content rises above 1 at. %, then the trend reverses rapidly and Ni doped skutterudites show rather poor ZTs.

For p-type skutterudites, elements with a lower number of electrons are chosen in order to create holes and strengthen p-type conduction; therefore, Fe/Co substitution is a successful route. Unfilled p-type skutterudites are unstable compounds; therefore, it is necessary to stabilize the structure by introducing fillers. Morelli et al. [17] in 1995 demonstrated that effect with $Ce_yFe_xCo_{4-x}Sb_{12}$ which was confirmed by Fleurial et al. [65]. Tang et al. [66] combined Fe/Co substitution with Ba, Ce, and Y as fillers; however, ZT did not surpass 1.1 at that time. With a well-evaluated Fe/Co ratio (for $E_yFe_xCo_{4-x}Sb_{12}$, $x \sim 3$) [60] in combination with double and multi-filling [59–61], ZT reached 1.2.

Another approach is doping at Sb site, which influences the electronic structure; deforms the pnictogen ring, which dominates over the spectrum of κ; and introduces defects, although resulting in lower κ. Single doping with Te [27, 67–73], Ge [29, 74, 75], Bi [76], and Sn [29, 75, 77, 78], as well as double doping Te + Ge [79] or Te + Sn [80–82] at Sb site, proved to be successful. Liu et al. [80], in addition to double doping with Te/Sn and Te/Ge, tried also Te/Si, and Te/Pb; however, Si and Pb did not embed into the skutterudite lattice. Khan et al. [83] created a porous microstructure for double-doped Te/Si $CoSb_{2.75}Si_{0.075}Te_{0.175}$, containing nano- to microsized irregularly shaped and randomly oriented pores, which created rattling features and reduced tremendously κ_L, yielding the highest ZT = 1.7, ever reported for an unfilled skutterudite.

In many cases, doping at Sb site was combined with Fe/Co and Ni/Co doping. An overview is presented in [6]; the highest ZT = 1.3 at 820 K was reached for $Fe_{0.2}Co_{3.8}Sb_{11.5}Te_{0.5}$ [76] and ZT = 1.1 at 725 K for triple-doped $Co_{3.9}Ni_{1.1}Sb_{11.5}Te_{0.4}Se_{0.1}$ [84].

The combination of doping and filling can, of course, further increase in ZT. Zhang et al. [75] presented ZT = 1.1 at 700 K for $Nd_{0.6}Fe_2Co_2Sb_{11.7}Ge_{0.3}$, an enhancement of almost 60% in comparison to the starting alloy without Ge. Rogl et al. enhanced ZT = 1.1 of $DD_{0.60}Fe_{2.8}Co_{1.2}Sb_{12}$ to ZT = 1.3 at 775 K in $DD_{0.59}Fe_{2.7}Co_{1.3}Sb_{11.8}Sn_{0.2}$ [29].

9.5.2 *Phonon Engineering*

The Nano-effect (HM, BM, HBM, HPT)

Based on the findings that nanostructuring can enhance ZT [23–25], researchers tried to realize these ideas experimentally. In polycrystalline materials, micro- and nanostructures were found to affect electrical and thermal properties [85–87] by lowering κ due to grain boundary scattering, however, simultaneously increasing ρ. It could be shown, e.g., by Nakagawa et al [88], Yang et al. [89], or Jie et al. [90], that the net effect was positive, which means that ball-milled samples exhibit higher ZTs than simply hand ground ones, although the post consolidation via hot pressing or spark plasma sintering induces grain growth.

In this context, it is important to mention that Short et al. [91], comparing hand ground and ball-milled *p*-type skutterudite samples with extended X-ray absorption Fi(EXAFS) analysis, could prove that via ball milling, no damage to the crystal lattice of nanoparticles is done and, therefore, even smaller particles could be used to further improve ZT.

Rogl et al. [31] compared physical properties of *p*- and *n*-type skutterudites, fabricated from the same *p*- and *n*-type skutterudite powders and hot-pressed in exactly the same way but using three different particle sizes (150, 100, 50 μm) as starting material and for the smallest particle size three different ball milling conditions. It turned out that the grain and crystallite size had no influence on lattice

vibrations as shown in Raman spectra; however, it was confirmed that the smaller the grain sizes, the higher is the TE performance due to a reduction of κ_L. ZT of *p*-type $DD_y(Fe_{1-x}Co_x)_4Sb_{12}$ was enhanced from ZT ~ 1.1 to ZT ~ 1.3 at 775 K and for *n*-type $(Mm,Sm)_yCo_4Sb_{12}$ from ZT ~ 1.0 to ZT ~ 1.6 at 825 K.

Another approach to reduce crystallite size and at the same time to increase in quantity of lattice defects and dislocations and, thereby, increase in the scattering of heat-carrying phonons is to apply severe plastic deformation (SPD) via high-pressure torsion (HPT) [92–101]. HPT-treated samples show reduced σ, almost unchanged S, and significantly reduced κ, which as net effect increases in ZT. Repeated heating or annealing during measurement cycles did not remove completely the beneficial microstructure achieved via HPT. The best results are ZT = 1.6 at 800 K for *p*-type $DD_{0.6}Fe_3CoSb_{12}$ (after temperature cycling ZT = 1.5) [96, 99] and ZT = 1.9 at 835 K for $Sr_{0.09}Ba_{0.11}Yb_{0.05}Co_4Sb_{12}$ (after temperature cycling ZT = 1.8) [98]. It must be noted that temperature-cycled samples are stable in respect to further cycling or annealing processes. The grain refinement due to SPD in addition infers a mechanical strengthening of the material as will be discussed in section 9.6.

Influence of Nanoprecipitates

A successful route to enhance ZT is to incorporate nanoparticles within bulk materials forming nanocomposites. By this approach, interfaces are built within bulk material, which should act in two ways: it should reduce κ more than σ by interface scattering and should increase S by energy filtering of charge carriers or by quantum confinement more than decreasing σ. The outcome is not only an increase in power factor, $PF = S^2\sigma$, but in ZT as well. As these nanocomposites might influence the charge carriers, nanoparticles must be selected, which enhance phonon scattering but do practically not disturb the charge carriers. In addition, with introduction of nanoparticles, the number of interfaces increases, and, eventually, impurity phases are introduced, reducing κ_L due to acting as scattering centers for phonons.

Various methods were employed to introduce the additive into the matrix, like solid-state or chemical-thermal reaction, chemical alloying methods, hydrothermal synthesis, in-situ reaction, sol-gel method, freeze-drying, melt milling, thermal diffusion, solvo-thermal method, and cryogenic grinding technique. However, in most cases the respective amount of additive was mixed (manually, via ball milling, BM, or high-energy ball milling, HBM) with the powder of the host material prior to hot pressing or spark plasma sintering. Also, chosen additives varied. A large group of additives comprises oxides (Al_2O_3, TiO_2, Cu_2O, ZnO, ZrO_2, MoO_2, WO_2, WO_3, Yb_2O_3, $La_{1.85}Sr_{0.15}CuO_4$, $BaFe_{12}O_{19}$) and the other one tellurides (PbTe, WTe_2, Bi_2Te_3, $AgSbTe_2$, $(Ag_2Te)_{0.40}(Sb_2Te_3)_{0.60}$, $(Ag_2Te)_{0.42}(Sb_2Te_3)_{0.58}$, $Co_4Sb_{11.5}Te_{0.5}$) or antimonides (InSb, NiSb, GaSb, $CoSb_3$ or simply excess of Sb). Some researchers dealt with metals (Ni, Ag, Co), borides ($Fe_{0.25}Co_{0.75}B$, $Ta_{0.8}Zr_{0.2}B$), nitrides (TiN), or silicides (Fe_3Si) as additives. Also, carbon-related materials (carbon fibers, multi-

or single-wall carbon nanotubes, reduced graphene oxide nanolayers, graphene, fullerenes) were introduced in the skutterudite matrix. A detailed description of the aforementioned methods and additives is given in a recent review ([102] and refs. therein).

Generally, it turned out that, independent of the chosen additive and preparation method, small amounts of additives, e.g., less than 2 wt. %, could enhance ZT more than bigger amounts. It can be noted that in almost 90% of all investigations, at least one sample with nanoprecipitates resulted in ZT enhancement, although in many cases the enhancement is within the error bar. However, the influence on mechanical properties was remarkable, as will be discussed in Sect. 9.6.

Most investigations were performed on *n*-type skutterudites, but here, selected examples of outstanding results will be discussed only. For many investigations $Yb_yCo_4Sb_{12}$ or $Ba_yCo_4Sb_{12}$ was used as matrix. ZT of $Yb_yCo_4Sb_{12}$ could be enhanced by 5–44% by adding either reduced graphene oxide layers [103] or multiwall carbon nanotubes [104] or Yb_2O_3 [105–107] reaching ZT values of ZT = 1.51, 1.43, 1.18, 1.16, 1.6, respectively. Rogl et al. [102], e.g., added excess Yb to $Sr_{0.09}Ba_{0.11}Yb_{0.05}Co_4Sb_{12}$ and found that Yb_2O_3 particles were formed and located at the grain boundaries of the matrix, as well as distributed within the grains as nanoscale inclusions: disturbing the phonon scattering, which reduced κ_L and enhanced ZT from 1.4 to 1.6. ZT was more than doubled with adding Ni as core shell particles [108] and almost tripled with $AgSbTe_2$, reaching ZT = 1.27 at 800 K [109]. The increased ZT was achieved by (a) enhanced mobility of charge carriers, which led to a threefold increase in σ, and (b) by enhanced S due to the energy filtering effect at interfaces between matrix and nanoinclusions, as well as (c) by reduction in κ. Adding Ag to $Ba_{0.3}Co_4Sb_{12}$ revealed 40% enhancement of ZT (Zhou et al. [110] and Peng et al. [111]). Here, a uniform dispersion of Ag nanoparticles was observed between grain boundaries and on grains' surfaces, leading to a large reduction in κ and a high ZT = 1.4 at 823 K. An even higher ZT enhancement, 44% and ZT = 1.3, was achieved for $Ba_yCo_4Sb_{12}$ with addition of fullerene [112]. Although Battabyal et al. [113] could triple ZT of $Ba_{0.4}Co_4Sb_{12}$, it still ended up with a rather low value of ZT = 0.9.

Much less was reported for *p*-type skutterudides as matrix; however, it is worth mentioning that for $CeFe_3CoSb_{12}$, ZT was raised from 1.05 to 1.22 (16%) with MoO_3 as additive [114] and even more, 50%, when Zhou et al. [115] added magnetic $BaFe_{12}O_{19}$. A quite meager ZT enhancement was reported for $CeFe_4Sb_{12}$ on addition of carbon fibers [116] or for $Ce_{0.85}Fe_3CoSb_{12}$ on addition of reduced graphene oxide layers [117] (8%) or for $DD_yFe_3CoSb_{12}$ with addition of $Ta_{0.8}Zr_{0.2}B$ (7%), in the latter case reaching ZT = 1.31 at 823 K [118].

Figure 9.2 shows a transmission electron microscopy (TEM) image as example. It shows how besides grains with sizes of about 200 nm two additional types of particles are present, bigger ones at the grain boundaries and smaller ones (smaller than 10 nm) inside the grains. These small grains provide more intensive phonon scattering and reduce κ_L, which results in ZT enhancement.

ZT values of $CoSb_3$ could be enhanced up to 60% with various additives, e.g., from ZT = 0.26 to 0.61 (graphene) [119], from 0.14 to 0.23 (fullerene) [51], from

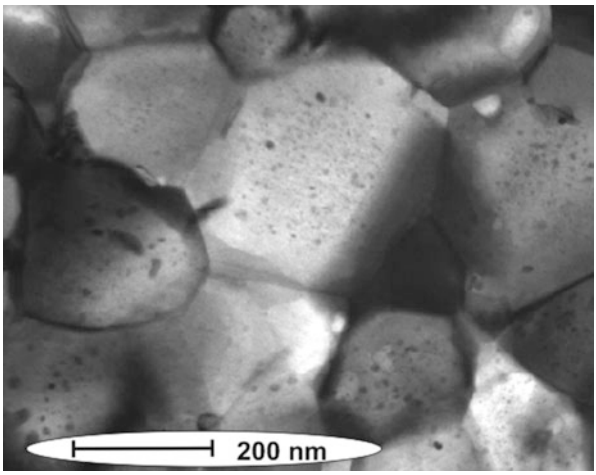

Fig. 9.2 TEM image of $DD_yFe_3CoSb_{12}$ with addition of 1 wt. % of $Ta_{0.8}Zr_{0.2}B$

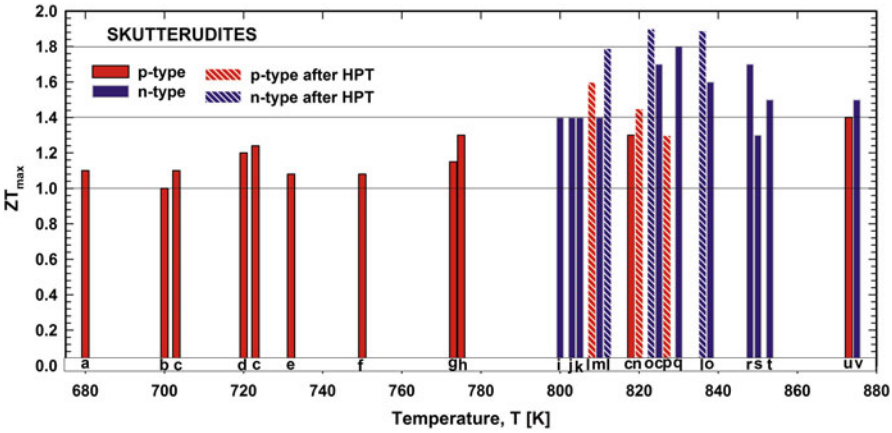

Fig. 9.3 Dependence of maximum ZT (ZT_{max}) of skutterudites on temperature. **a** - [48], **b** - [123], **c** - [102], **d** - [59], **e** - [90], **f** - [66], **g** - [124], **h** - [29], **i** - [93], **j** - [125], **k** - [126], **l** -[97], **m** - [127], **n** - [29], **o** - [98], **p** - [76], **q** - [128], **r** - [54], **s** - [129], **t** - [130], **u** - [65], **v** - [131]

0.25 to 0.4 (WO_2) [114], or from 0.45 to 0.71 by simply mixing micropowder of $CoSb_3$ with nanopowder of $CoSb_3$ [120].

Zhao et al. [121] and Tan et al. [122] used as matrix unfilled skutterudites $Co_4Sb_{11.7}Te_{0.3}$ and $FeSb_{2.2}Te_{0.8}$, respectively. Zhao added WO_3 and could raise ZT from 0.44 to 0.65 (48%), whereas Tan added InSb, but the rise was only 17%.

Fig. 9.3 shows an overview of the highest ZT values in dependence on the peak temperature. Generally seen, high ZT values of *p*-type skutterudites (higher than 1, reaching 1.3) are lower than ZT values of *n*-type skutterudites (higher than 1.3, reaching 1.8); in addition, maxima of *p*-type skutterudites occur at lower temperatures than those of *n*-type skutterudites. There are two exceptions: the maximum ZT

with additives can be shifted to higher temperatures (818 K) and ZT of $CeFe_4Sb_{12}$, published by Fleurial in 1996, which for *p*-type skutterudite had a very high ZT = 1.4 at 900 K; however, this value could, so far, not be reproduced.

After SPD via HPT, *p*- and *n*-type skutterudites show enhanced ZT values as discussed in Sect. 9.5.2.1. above.

9.6 Mechanical Properties

As the authors provided a summary on mechanical properties of skutterudites in two articles [132, 133] and a review article [134], as well as an update [13], we will give here only a short overview but will explain the changes of mechanical properties under various influences in more details.

Generally, mechanical properties are dependent on various parameters such as (1) the sample's synthesis method and (2) the sample's composition, (3) surface preparation, as well as (4) grain size. Mechanical properties, furthermore, are strongly dependent on density/porosity and temperature. In addition, the used equipment can influence the values as, e.g., with resonant ultrasound spectroscopy, the whole sample is excited, whereas, with micro- or nanoindenter, only a very small area of the sample is measured. Usually, a difference exists between static hardness (measured with microhardness tester, where the imprint is measured after the force is released and the imprint has contracted) and dynamic hardness (measured with micro- or nanoindenter directly, while the load is applied). In addition, one has to consider that DFT calculated data refer always to samples with ideal structure at a temperature of zero Kelvin.

Average values of the crystallite size of *p*- and *n*-type skutterudites after hot pressing are about 150 nm. After HPT these sizes are decreased to about one third (~40–50 nm) and after measurement-induced heating or after annealing, crystallites grow slightly but never reach the size of the starting material. These important changes are accompanied by changes of (1) dislocation density (starting material, $\sim 3 \times 10^{13}$ m^{-2}; HPT: $\sim 2 \times 10^{14}$ m^{-2}; after annealing, $\sim 1.5 \times 10^{14}$ m^{-2}), (2) lattice parameter (slightly enhanced after HPT and a bit reduced after annealing), and (3) relative density (slightly lower after HPT and growing almost back to the starting values after annealing) [97, 133, 134].

Vickers hardness (HV) values for hand ground samples equal to HV0.1 = 240–300 for *p*-type and HV0.1 = 300–400 for *n*-type skutterudites are, due to bigger grain sizes and lower densities, lower than the values of ball-milled *p*- and *n*-type skutterudites with relative densities in the range of 89–99%, which, with one or two outliers, are HV0.1 = 430–530 and HV0.1 = 500–600, respectively. These values document that, generally, *n*-type skutterudites are harder than *p*-type counterparts.

Although after SPS via HPT, the relative density of samples is slightly decreased, following Hall-Petch relation (the smaller the crystallite size, the harder the alloy), hardness is enhanced [97]. HPT processed samples are not homogeneous with

respect to shear strain, $\gamma = (2\pi Nr)/t$ (where N is number of revolutions, r is radius, and t is thickness of the sample) with $\gamma \sim 39$ at the rim and $\gamma \sim 8$ at the center of the sample (for r=10 mm, t=1 mm). Therefore, hardness values decrease from the rim to the center area, e.g., for $DD_{0.6}Fe_3CoSb_{12}$ from HV0.1 = 580 to HV0.1 = 440 for ball-milled sample, with hardness of HV0.1 = 410 before HPT [100]. Although samples, annealed for 1 h, show no changes in density or hardness, those annealed for 24 h at 673 K slightly soften (about 1% decrease), but do not show changes after further annealing.

Nanoparticles distributed evenly at the grain boundaries may influence mechanical properties significantly. With addition of borides and oxides, density of the samples increases slightly. Concerning hardness, the additives can strengthen or soften the material. As can be seen in Fig. 9.4, *p*- and, especially, *n*-type skutterudites have much higher hardness values (up to 50%) with addition of borides. The more boride is added, the harder the material, but ZT decreases as reported in ref. [102]. Addition of oxides, however, softens the skutterudites.

Young's modulus, E, of ball-milled skutterudites at room temperature and for relative densities above 95% ranges from 120 GPa to 135 GPa for *p*-type and is a little bit higher, 130 GPa to 145 GPa, for *n*-type skutterudites [133]. Fig. 9.4 shows the relation between hardness and Young's modulus. A linear fit to all ball-milled samples (Fig. 9.4) reveals the relation HV = 3.75(16)E. Only some data are beyond the error bar, and, of course, the data for hand ground samples are much lower. It is obvious that all HV - E data for samples with added borides are enhanced and lay

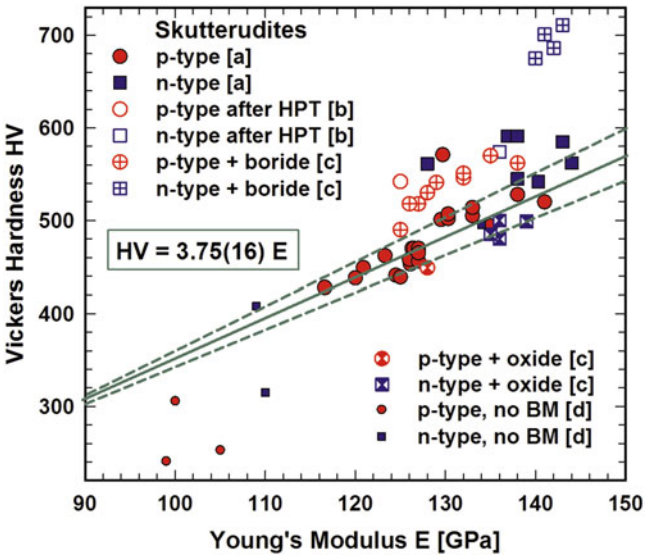

Fig. 9.4 Young's modulus vs. Vickers hardness of *p*- and *n*-type hand ground (small symbols) and ball-milled (large symbols) skutterudites before and after HPT or with addition of nanoprecipitates. **[a]** - [134] and refs. therein, **[b]** - [97], **[c]** - [102] and refs. therein, **[d]** - [134]

outside of the fit region, for *n*-type much more than for *p*-type. The values decrease after an oxide was added. For HPT processed samples, exemplarily, one value for *p*- and *n*-type is displayed and shows enhancement as already discussed.

As HPT processed samples are brittle and available in small disks only, it is not easy to study other mechanical properties except hardness and elastic moduli.

Compressive strength and flexural strength of $CoSb_3$ and of Sb-substituted unfilled and filled skutterudites were investigated [102] and appear enhanced with addition of oxides [135, 136], carbon fibers [116], or titanium nitride [71, 137] but reduced with addition of multiwall carbon nanotubes [138]. The authors saw an increase in compressive strength of *p*-type $DD_yFe_3CoSb_{12}$ from 450 MPa to 520 MPa after 5 wt. % of borides was added.

Fracture toughness, K_C, (or fracture resistance, in case it was determined from crack lines propagating out of hardness imprints) follows the behavior of compressive and flexural strength. With the addition of borides, K_C is enhanced [71, 116, 136], e.g., for $DD_yFe_3CoSb_{12}$ from 1.6 to 1.9 MPa $\times$ $m^{1/2}$ or for $(Mm,Sm)_yCo_4Sb_{12}$ from 1.8 to 2.0 MPa $\times$ $m^{1/2}$. However, multiwall carbon nanotubes decrease flexural strength and K_C as well [138].

According to Ashby plot [139] of elastic modulus vs. hardness, as shown in Fig. 9.5, skutterudites are located between TAGS (Te - Ag - Ge - Sb), Bi_2Te_3, and LAST (Pb - Ag - Sb - Te) TE materials and ceramics. The ratio of hardness to elastic moduli is higher for skutterudites than for metals and steels.

In order to avoid stresses on *p* and *n* legs of TE modules during repeated heating and cooling cycles, parameters of mechanical properties, especially, of thermal

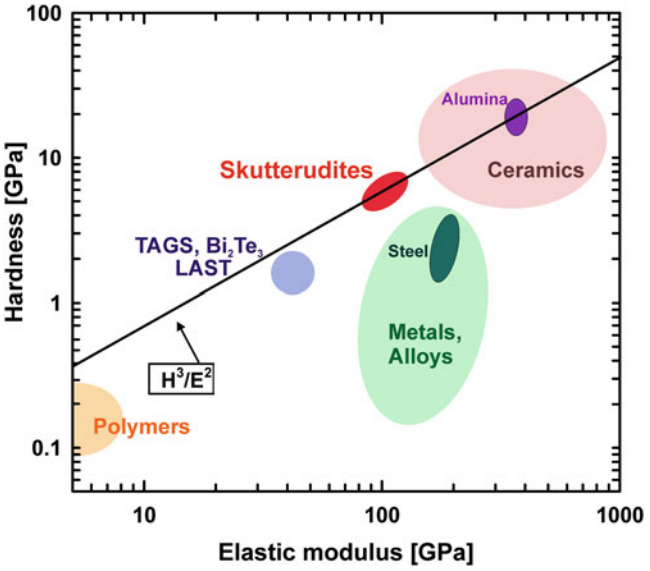

Fig. 9.5 Ashby plot of elastic modulus vs. hardness including Te-based thermoelectrics and skutterudites

expansion coefficients α, should not differ much. Generally, Sb-based filled *p*-type skutterudites ($\alpha_{av} = 11.2 \times 10^{-6}\ K^{-1}$) have higher coefficients of thermal expansion than *n*-type counterparts ($\alpha_{av} = 9.6 \times 10^{-6}\ K^{-1}$) (see detailed investigation of the expansion behavior of skutterudites [140]). For Fe/Ni-substituted multi-filled skutterudites, it was possible to get almost the same α for *p*-type, $Ba_{0.15}DD_{0.28}Yb_{0.05}Fe_3NiSb_{12}$, α(300–800 K) $= 11.8 \times 10^{-6}\ K^{-1}$ and *n*-type, $Ba_{0.09}Sr_{0.02}DD_{0.22}Yb_{0.02}Fe_{2.4}Ni_{1.6}Sb_{12}$, α(300–800 K) $= 11.9 \times 10^{-6}\ K^{-1}$) [141]; however, both materials have ZT ≈ 1 only.

Using another approach, Rogl et al. [118] have demonstrated that borides dispersed in both *p*-type $DD_{0.7}Fe_3CoSb_{12}$ and *n*-type $(Mm,Sm)_yCo_4Sb_{12}$ can level out the discrepancy in α. By adding either 1.5 or 20 wt. % $Ta_{0.8}Zr_{0.2}B$ or adding 5 wt. % $Fe_{2.25}Co_{0.75}B$ to $DD_{0.7}Fe_3CoSb_{12}$, α could be reduced from α(300–800 K) $= 11.3 \times 10^{-6}\ K^{-1}$ to α(300–800 K) $= 10.6 \times 10^{-6}\ K^{-1}$, α(300–800 K) $= 10.4 \times 10^{-6}\ K^{-1}$ or α(300–800 K) $= 9.7 \times 10^{-6}\ K^{-1}$, respectively. On the other hand, $Ta_{0.8}Zr_{0.2}B$ (1 wt. %) dispersed in $(Mm,Sm)_yCo_4Sb_{12}$ enhanced α from α (300–800 K) $= 9.65 \times 10^{-6}\ K^{-1}$ to α(300–800 K) $= 10.5 \times 10^{-6}\ K^{-1}$. Considering ZT changes accompanying nanodispersions, luckily for *n*-type, ZT is higher with the addition of $Ta_{0.8}Zr_{0.2}B$. For *p*-type with 1.5 wt. % $Ta_{0.8}Zr_{0.2}B$, ZT is, within the error bar, almost the same (ZT = 1.23 and ZT = 1.26, respectively).

It should be mentioned that $La_{1.85}Sr_{0.5}CuO_4$ has the reverse effect, as it was also the case for hardness and Young's modulus; it enhances α of *p*-type and lowers α of *n*-type material. Ashby plot [139] of α vs. κ (Fig. 9.6) shows that skutterudites have

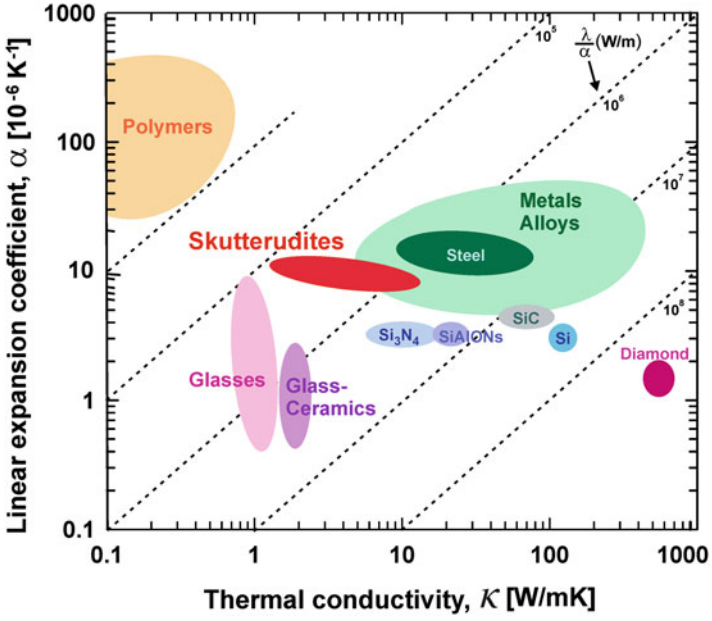

Fig. 9.6 Ashby plot of thermal conductivity, κ, vs. thermal expansion coefficient, α

thermal expansion coefficients in the range of metals, lower than polymers but higher than glasses; however, the thermal conductivity is mainly lower than that of metals.

The length change of HPT processed *p*- and *n*-type skutterudites is strange and could not be explained completely so far. Fact is that the measurements from 4.2 K to room temperature performed with a capacitance dilatometer, using the tilted plate principle, do not show, within the error bar, any discrepancies compared to unprocessed reference material. Above room temperature, using the zero-force method with a thermomechanical analyzer, a strange behavior appears. In the temperature range of 300–400 K, the graph of the length change vs. temperature is prolonged, but with increasing temperature, it becomes slightly less steep, as shown for $DD_{0.44}Fe_{2.1}Co_{1.9}Sb_{12}$ (Fig. 9.7) as an example. In case of $DD_{0.44}Fe_{2.1}Co_{1.9}Sb_{12}$, at about 450 K, a kink appears, and the sample contracts and afterward expands again but much more than prior to the compression and almost in the range of glass-ceramics, which is in favor of a high ZT.

This behavior was observed for all HPT processed skutterudites; however, the kink varies in temperature. It seems that during measurement-induced annealing, defects heal out, and/or internal microcracks fuse together, and stresses die down. After the first heating, the curve for decreasing temperature, as well as cycling, shows a linear expansion behavior without any kink. The value of α, before and after HPT processing in the low temperature range, is the same (for $DD_{0.44}Fe_{2.1}Co_{1.9}Sb_{12}$ $\alpha(115–300\ K) = 11.7 \times 10^{-6}\ K^{-1}$). For the sample before HPT, this value does not change in the high temperature range and is, within the error bar, the same as for the HPT processed sample after heat treatment (for $DD_{0.44}Fe_{2.1}Co_{1.9}Sb_{12}$ α

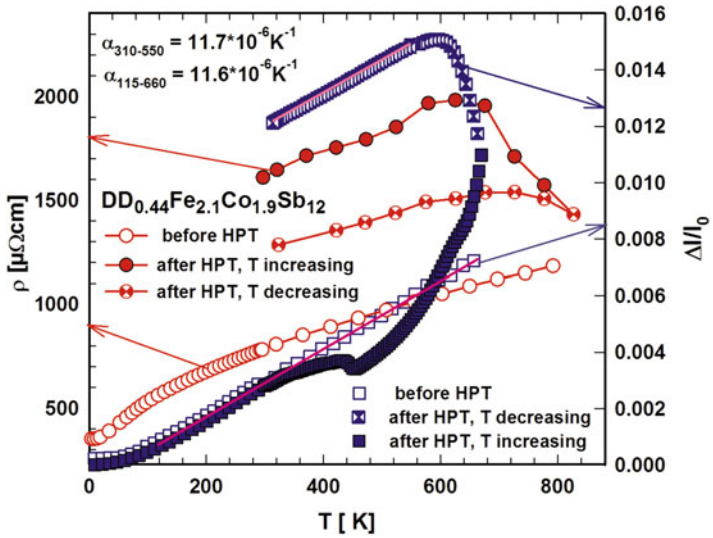

Fig. 9.7 Temperature-dependent electrical resistivity ρ (left scale) and thermal expansion $\Delta|l|_0$ of $DD_{0.44}Fe_{2.1}Co_{1.9}Sb_{12}$ before and after HPT. Pink lines display the linear fit to $\Delta|l|_0 - T$ curve

(115–300 K) = 11.7 × 10^{-6} K^{-1}). It is interesting to note that ρ (Fig. 9.7) of HPT processed sample, although much higher than that of the reference sample, starts to decrease at about the same temperature where the kink in thermal expansion appears. In parallel to the thermal expansion, the resistivity measurement with decreasing temperature and further measurements do not reveal any kink.

All these changes in mechanical properties and thermal expansion show how flexible skutterudites are, as one can adjust those to the needs of any application, although in some cases these changes may be connected with a damage of ZT.

9.7 Thermal Stability, Sublimation, and Oxidation

As thermal stability and oxidation of any thermoelectric material is a crucial point for its application, it is necessary to investigate it, also for Sb-based skutterudites. In 2017 Rogl et al. [13] published a table with all known oxidation onset temperatures and activation energies.

Caillat et al. [142] in 2004 were first to investigate long-term stability of $CoSb_3$ as bulk in dynamic vacuum (10^{-4} Pa) and found a decomposition into $CoSb_2$ and CoSb with the sublimation of Sb at 575 °C. They saw that time-dependent weight losses follow a parabolic-like behavior. Later (2011) Zhao et al. [143] confirmed such behavior when analyzing time-dependent mass losses of spark plasma sintered $CoSb_3$ in vacuum in the temperature range of 600–750 °C. They evaluated vaporization kinetics of Sb and took it as decomposition of $CoSb_3 \rightarrow CoSb_2 + Sb$. In addition, they saw a decrease in ZT from 0.24 to 0.16 at 327 °C after a thermal test duration of 16 days. At the same time, Leszczynski et al. [144], using powder samples and employing non-isothermal differential analysis and thermography, reported 420 °C as start of decomposition. In the same temperature range, oxidation of $CoSb_3$ thin films (380 °C) was reported by Savchuk et al. [145]. However, for Fe/Co-substituted alloys, oxidation starts earlier, with 300 °C. Wojciechowski et al. [146] observed the same oxidation temperature (380 °C) for $CoSb_3$ as well as for $CoSb_3$ with 1.5 at. % Te. Zhao et al. [147] reported surface antimony oxide layers, as soon as skutterudites are exposed to air at temperatures above 400 °C. At 600 °C, they even found two layers, which continue to grow. Park et al. [148] reported that no oxide layers formed in vacuum even after 120 h annealing at 550 °C.

Peddle et al. [149] observed the onset of oxidation of $EuFe_4Sb_{12}$ at 360 °C, whereas of $EuRu_4Sb_{12}$ at 460 °C. The same tendency was observed by Sigrist et al. [150] with an oxidation temperature of $CeRu_4Sb_{12}$ (470 °C), being more than 100 °C higher than that of $CeFe_4Sb_{12}$ and 70 °C higher than that of $CeRu_3CoSb_{12}$. The conclusion of these observations is that oxidation resistance increases with the content of noble elements.

Generally, activation energies for the oxidation of Co-based skutterudites (105–270 kJ/mol) are higher than those for rare earth-filled Fe-based skutterudites (14–40.5 kJ/mol), which can be due to the high oxygen affinity of rare earth atoms resulting in metastable Fe_4Sb_{12} that decomposes into $FeSb_2$ and Sb, accelerating the

oxidation rate [13, 151]. In addition, for $CoSb_3$-based *n*-type skutterudites, a reduction in oxidation resistance was observed with the increase in the rare earth content by Xia et al. [152] for $Yb_yCo_4Sb_{12}$; however, Park et al. [148, 153] saw an opposite influence of the filler for $In_{0.25}Co_3MnSb_{12}$ and $In_{0.25}Co_3FeSb_{12}$, blaming it on the formation of InSb.

In any case protecting the skutterudite surface with an inert material can prevent oxidation processes.

Sklad et al. [154] and Xia et al. [151] studied the oxidation behavior of the filled *p*-type skutterudite $CeFe_4Sb_{12}$ and reported oxidation temperatures of 300 and 327 °C, respectively. In addition, Xia et al. found that below 800 K, an oxide layer of Sb_2O_3, Sb_2O_4, Ce_2O_2Sb, and amorphous Fe^{3+} oxide forms. At temperatures above 527 °C, an additional layer comprising amorphous Ce, $FeSb_2$, and Sb evolves beneath the first one, proving that oxidation is accompanied by decomposition of $CeFe_4Sb_{12}$. They calculated the activation energy of the oxidation of 4.0 kJ/mol (427–527 °C). Qiu et al. [155] observed about the same for $Ce_{0.9}Fe_3CoSb_{12}$, which has an oxidation temperature of 377 °C. Shin et al. [156] reported for $La_{0.3}Fe_3CoSb_{12}$ an only slightly higher oxidation temperature 400 °C.

Broz et al. [157, 158] investigated recently the thermal and phase stability of ball-milled and hot-pressed bulk $CoSb_3$ skutterudite by means of differential thermal analysis (DTA) and Knudsen effusion mass spectrometry (KEMS) accompanied by scanning electron microscopy. KEMS measurements (at 589, 618, and 637 °C) (Fig. 9.8) agree well with the diffusion profiles showing that Sb evaporation from $CoSb_3$ is a complex kinetic process including initial evaporation of free or weakly bound Sb (obviously excess Sb, from the material) followed by temperature-dependent Sb depletion resulting in phase transformations $CoSb_3 \rightarrow CoSb_2 \rightarrow CoSb \rightarrow \alpha(Co)$. However, structure stability up to ~620 °C was confirmed. Above 640 °C, $CoSb_2$ forms on the sample's surface (see insert in

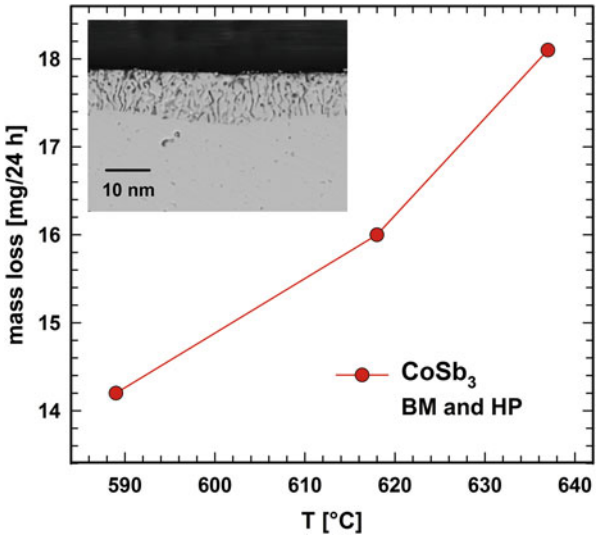

Fig. 9.8 Temperature-dependent mass loss in mg per 24 h for BM (ball milled) and HP (hot-pressed) bulk $CoSb_3$ in vacuum. Insert: SEM micrograph of the surface layer at 637 °C

Fig. 9.8), which might grow with further increase of temperature. With low mass losses of Sb, as found from KEMS measurements (Fig. 9.8), $CoSb_3$ can be considered as stable basis for TE materials as long as it is used in protective atmosphere and below 600 °C.

In our recent review [13], we described a lot of effort in thermal stability tests, using commercially hot-pressed samples, as well as hot-pressed samples under laboratory conditions, in both cases from commercial *p*- and *n*-type skutterudite powders ($DD_yFe_3CoSb_{12}$ and $(Mm,Sm)_yCo_4Sb_{12}$), produced in Austria. From hot-pressed disks, samples were cut of various shapes and sizes, in parallel and perpendicular to the pressing direction, and room temperature electrical resistivity, as well as weight, was measured. Then the couples of *p*- and *n*-type material, as well as individual *p*- and *n*-type materials, were sealed in evacuated and Ar-filled quartz ampoules (length 40 cm). TE material was placed at the hot end of the ampoule, which was subjected to a temperature gradient $T_{hot} = 600$ °C and $T_{cold} = 80$ °C. About every 30 days, weight and electrical resistivity of the samples were controlled. After 504, 768, 2475, 4363, and 8800 h, the samples were quenched and investigated by SEM, EPMA (electron probe microanalysis), and XRD (X-ray diffraction), and, particularly, TE properties and those of the reference samples were measured in the temperature range from 300 K to 850 K. It turned out that for *n*-type reference samples, no differences in TE properties occurred; samples had ZT = 1.2 at 800 K. However, for the commercial hot-pressed *p*-type sample, secondary phases were detected, resulting in a lower ZT of 0.9 in comparison to laboratory hot-pressed samples with ZT = 1.1 at 800 K.

Summing up the long-term stability study [13], we can state the following: (1) long-term thermal stability tests at 600 °C show that Ar pressure had a beneficial effect on the suppression of Sb evaporation as compared to experiments in vacuum; (2) *p*-type materials show stronger Sb evaporation, which occurs in the surface zone, resulting in weight loss; (3) unusual weight exchange between *p* and *n* legs occurred for commercial hot-pressed samples, attributed to partial oxidation of *p*-type material; and (4) ZT at 800 K remains in the range of 0.9 for *p*-type but decreases from 1.2 to 1.0 for *n*-type, which was attributed to a decrease in the filling level from $y = 0.17$ to $y = 0.11$.

Generally, one can conclude that coating or encapsulation under argon is a necessity for long-term stability in order to prevent oxidation and/or sublimation. The optimal coating should have a low thermal and electrical conductivity, should be chemically inert, and should have good adhesion to the substrate and a thermal expansion coefficient as close as possible to that of the skutterudites.

9.8 Large-Scale Production of Skutterudite Material: Modules and TE Generators

The goal to develop high ZT skutterudites in laboratory has been very well achieved. Combining (1) the right fillers in (2) the right proportion with (3) substituting at Co site and/or Sb site together with (4) a well-developed preparation method to achieve

dense samples with small grains leads already to spectacular ZT values and respective leg efficiencies: for *p*-type $DD_{0.59}Fe_{2.7}Co_{1.3}Sb_{11.8}Sn_{0.2}$ ZT = 1.3 with η(300–800 K) = 14.3% [29] and for *n*-type $(Sr, Ba, Yb)_yCo_4Sb_{12}$ + 9.1 wt. % $In_{0.4}Co_4Sb_{12}$ ZT = 1.8 with η(300–800 K) = 17.5% [127]. To our knowledge, these are currently the highest values. As described in Sect. 9.5.2.1., these values can be further enhanced applying severe plastic deformation via high-pressure torsion.

All these high ZT values with high leg efficiencies, thermal stability, and proper mechanical properties are useless, as long as samples can only be produced in grams. Therefore, it is a big step forward that the commercial production of skutterudites powders has started. After many tests, industrial manufacturers have developed *p*- and *n*-type skutterudite powders, which have, after hot pressing, respectable ZT values at 800 K, i.e., ZT = 1.1 ± 0.1 for *p*-type and ZT = 1.3 ± 0.1 for the *n*-type. These values can be enhanced to ZT = 1.3 and ZT = 1.6, respectively, via ball milling under well-defined conditions [31, 32] prior to hot pressing. Nong and Hung [159], as well as Pryds [160], could confirm these outstanding results.

In a review article, Aswal et al. [161] present various highly efficient TE modules based also on skutterudites. It is well known that segmented modules, using skutterudites and other TE compounds, can reach high efficiencies like η = 15% (with temperature gradients of 1000 to 152 °C and 700 to 27 °C) [162] or calculated values of even 18% [163]; however, for mass production these segmented modules are not suitable. Therefore, it is notable that non-segmented, skutterudite-based modules reach already efficiencies of η = 7% (gradient of 500 to 40 °C) [164], η = 9% (gradient of 550 to 70 °C) [165], and even η = 10% (gradient of 550 to 90 °C) [166]. Durability tests performed by Ochi et al. [167] under thermal cycling from 200 °C to 600 °C for 8000 h on modules have shown that the power output decreases by 9.5% with simultaneous increase in module's resistance by 6.6%.

Pryds [160] built a TE generator based on commercial skutterudite powders, ball milled and hot-pressed according to evaluations presented in [31], and reached an efficiency of 11.2% for a temperature gradient of 533 K. Kober [168] used the same industrial starting material (hot-pressed only) and built a TE generator with an efficiency of almost 8% (temperature gradient equals to 480 K) with small dimensions (smaller than 3 dm^3) and a mass below 8 kg.

9.9 Conclusion

We guided the reader through the various steps of developments of skutterudites concerning thermoelectric behavior, stability, mechanical properties, and thermal expansion. With high ZT values for *p*- and *n*-type skutterudites, synthesized in the laboratory, as well as produced in large quantities, with sufficiently strong mechanical parameters and almost the same coefficient of thermal expansion for *p*- and *n*-type materials, we dare to say: yes, it is a breakthrough. Technological applications of skutterudite thermoelectrics for thermoelectric power generation are ready to start, given a large-scale module producer.

References

1. H.S. Kim, W. Liu, G. Chen, C.-W. Chu, Z. Ren, PNAS **112**(27), 8205 (2015)
2. G.S. Nolas, D.T. Morelli, T.M. Tritt, Ann. Rev. Mater. Sci. **29**, 89 (1999)
3. C. Uher, Sem. Ther. **69**(5), 139 (2001)
4. G.J. Snyder, E.S. Toberer, Nat. Mater. **7**, 105 (2008)
5. A.J. Minnich, M.S. Dresselhaus, Z.F. Ren, G. Chen, Energ. Environ. Sci. **2**, 466 (2009)
6. M. Rull-Bravo, A. Moure, J.F. Fernández, S. Martín-González, RSC Adv. **5**, 41653 (2015)
7. G. Schierning, R. Chavez, R. Schmechel, B. Balke, G. Rogl, P. Rogl, Transl. Mater. Res. **2**, 025001 (2015)
8. R. Fitriani, B.D. Ovik, M.C. Long, M. Barma, M.F.M. Riaz, S.M. Sabri, S.R. Saidur, Renew. Sustain. Energy Rev. **64**(635), 659 (2016)
9. G. Rogl, P. Rogl, in: *Current Opinion in Green and Sustainable Chemistry* , ed. by S. Schorr, (IOP Publishing Bristol 2017) p. 50
10. D.M. Rowe, *Thermoelectrics Handbook Macro to Nano* (CRC Taylor&Francis, Boca Raton, FL, 2006)
11. D.M. Rowe, C.M. Bhandari, *Modern Thermoelectrics* (Reston Publishing Company, Reston, VA, 1983)
12. H.J. Goldsmid, *Introduction to Thermoelectricity*, vol 121, 2nd edn. (Springer, Berlin, Heidelberg, 2016)
13. G. Rogl, A. Grytsiv, E. Bauer, P. Rogl, *Advanced Thermoelectrics: Materials, Contacts, Devices and Systems*, ed. by Z. Ren, Y. Lan, Q. Zhang, (CRC Press, Boca Raton, FL, 2018) p.193
14. I. Oftedal, Z. für Kristallogr. **66**, 517 (1928)
15. A. Kjekshus, T. Rakke, Acta Chem. Scand. A **28**(1), 99 (1974)
16. L.D. Dudkin, N. Kh, Z. Abrikosov, Neorg. Khim. **2**(1), 12 (1957)
17. D.T. Morelli, T. Caillat, J.P. Fleurial, A. Borshchevsky, J. Vandersande, B. Chen, C. Uher, Phys. Rev. B Cond. Matter **51**(15), 9622 (1995)
18. T. Caillat, A. Borshchevsky, J.-P. Fleurial, J. Appl. Phys. **80**(8), 4442 (1996)
19. L. Bertini, K. Billquist, M. Christensen, C. Gatti, L. Holmgreen, B. Iversen, E. Mueller, M. Muhammed, *G.* Noriega, A. Palmqvist, D. Platzek, D.M. Rowe, A. Saramat, C. Stiewe, M. Toprak, S.G. Williams, Y. Zhang, in *Proceedings of the Twenty-Second International Conference on Thermoelectrics, ICT2003, IEEE Cat. No.03TH8726* (IEEE, Piscataway, NJ, 2003), pp. 117–120
20. W. Jeitschko, D.J. Braun, Acta Cryst. B **33**, 401 (1977)
21. G.A. Slack, V.G. Tsoukala, J. Appl. Phys. **76**, 665 (1994)
22. C. Uher, B. Chen, S. Hu, D.T. Morelli, G.P. Meisner, Symp. Mater. Res. Soc. **348**, 315 (1997)
23. L.D. Hicks, M.S. Dresselhaus, Phys. Rev. B **47**, 2727 (1993)
24. R. Venkatasubramanian, In: *Semiconductors and Semimetals*, ed. by T. Tritt (Academic Press, 2001, Nashua, NH vol. 71) p. 175
25. G. Chen, In: *Semiconductors and Semimetals*, ed. by T. Tritt (Academic Press, 2001, Nashua, NH vol. 71) p. 203
26. I. Kogut, S. Nickalov, V. Ohorodnichuk, A. Dauscher, C. Candolfi, P. Masschelein, A. Jackot, B. Lenoir, Acta Phys. Pol. A **133**(4), 879 (2018)
27. L. Deng, L.B. Wang, J.M. Qin, T. Zheng, J. Ni, X. Peng Jia, H. An Ma, Mod. Phys. Lett. B **29**, 1550095 (2015)
28. L. Guo, X. Xu, J.R. Salvador, Appl. Phys. Lett. **106**, 231902 (2015)
29. G. Rogl, A. Grytsiv, P. Heinrich, E. Bauer, P. Kumar, N. Peranio, O. Eibl, J. Horky, M. Zehetbauer, P. Rogl, Acta Mater. **91**, 227 (2015)
30. L. Zhang, A. Grytsiv, M. Kerber, P. Rogl, E. Bauer, M.J. Zehetbauer, J. Wosik, G.E. Nauer, J. Alloys Compd. **481**, 106 (2009)
31. G. Rogl, A. Grytsiv, P. Rogl, E. Bauer, M. Hochenhofer, R. Anbalagan, R.C. Mallik, E. Schafler, Acta Mater. **76**, 434 (2014)

32. A. Sesselmann, G. Skomedal, H. Middleton, E. Müller, J. Electron. Mater. **45**(3), 1397 (2016)
33. J.L. Feldman, D.J. Singh, N. Bernstein, Phys. Rev. B: Cond. Matter Mater. Phys. **89**(22), 224304 (2014)
34. M.M. Koza, M.R. Johnson, R. Viennois, H. Mutka, L. Girard, D. Ravot, Nat. Mater. **7**(10), 805 (2008)
35. M. Rotter, P. Rogl, A. Grytsiv, W. Wolf, M. Krisch, A. Mirone, Phys. Rev. B **77**(14), 144301 (2008)
36. W. Li, N. Mingo, Phys. Rev. B **89**, 184304 (2014)
37. T. He, J. Chen, H.D. Rosenfeld, M.A. Subramanian, Chem. Mater. **18**, 759 (2006)
38. L. Wang, K. Cai, Y. Wang, H. Li, H. Wang, Appl. Phys. A Mater. Sci. Process. **97**, 841 (2009)
39. Y. Zhang, C. Li, Z. Du, C. Guo, J.C. Tedenac, CALPHAD 33(2), 405 (2009)
40. V.V. Khovaylo, T.A. Korolkov, A.I. Voronin, M.V. Gorshenkov, A.T. Burkov, J. Mater. Chem. A **5**(7), 3541 (2017)
41. G.S. Nolas, H. Takizawa, T. Endo, H. Sellinschegg, D.C. Johnson, Appl. Phys. Lett. **77**(1), 52 (2000)
42. R.C. Mallik, J.-Y. Jung, V.D. Das, S.-C. Urband, I.-H. Kim, Solid State Commun. **141**(4), 233 (2007)
43. R.C. Mallik, J.-Y. Jung, V. Damodara Das, S.-C. Ur, I.-H. Kim, in *Proceedings of the Twenty-Fifth International Conference on Thermoelectrics* (ICT, Vienna, Austria, 2006), p. 431
44. C. Godart, E.B. Lopes, A.P. Goncalves, Acta Phys. Pol. A **113**, 403 (2008)
45. B.C. Sales, B.C. Chakoumakos, D. Mandrus, Phys. Rev. B **61**(4), 2475 (2000)
46. S. Choi, K. Kurosaki, Y. Ohishi, H. Muta, S. Yamanaka, J. Appl. Phys. **115**(2), 023702 (2014)
47. X. Li, B. Xu, L. Zhang, F. Duan, X. Yan, J. Yang, Y. Tian, J. Alloys Compd. **615**, 177 (2014)
48. L. Zhang, B. Xu, X. Li, F. Duan, X. Yan, Y. Tian, Mater. Lett. **139**, 249 (2015)
49. B. Chen, J.-H. Xu, C. Uher, D.T. Morelli, G.P. Meisner, J.-P. Fleurial, T. Caillat, A. Borshchevsky, Phys. Rev. B Cond. Matter **55**(3), 1476 (1997)
50. G.S. Nollas, J.L. Cohn, G.A. Slack, Phys. Rev. B **58**(1), 164 (1998)
51. X. Shi, L.D. Chen, J. Yang, G.P. Meisner, Appl. Phys. Lett. **84**, 2301 (2004)
52. Z.G. Mei, J. Yang, Y.Z. Pei, W. Zhang, L.D. Chen, J. Yang, Phys. Rev. B **77**, 045202 (2008)
53. L. Xi, J. Yang, W. Zhang, L. Chen, J. Yang, Am. Chem. Soc. **131**(15), 5563 (2009)
54. X. Shi, J. Yang, J.R. Salvador, M. Chi, J.Y. Cho, H. Wang, S. Bai, J. Yang, W. Zhang, L. Chen, J. Am. Chem. Soc. **133**, 7837 (2011)
55. X. Shi, W. Zhang, L.D. Chen, J. Yang, Phys. Rev. Lett. **95**, 185503 (2005)
56. J. Yang, W. Zhang, S.Q. Bai, Z. Mei, L.D. Chen, Appl. Phys. Lett. **90**(19), 192111 (2007)
57. Q.M. Lu, J.X. Zhang, X. Zhang, Y.Q. Liu, D.M. Liu, M.L. Zhou, J. Appl. Phys. **98**(10), 106107 (2005)
58. G. Rogl, A. Grytsiv, E. Bauer, P. Rogl, M. Zehetbauer, Intermetallics **18**, 57 (2010)
59. G. Rogl, A. Grytsiv, P. Rogl, E. Bauer, M. Zehetbauer, Intermetallics **19**, 546 (2011)
60. G. Rogl, A. Grytsiv, P. Rogl, E. Bauer, M. Zehetbauer, Solid State Phenom. **170**, 2435 (2011)
61. L. Zhang, A. Grytsiv, M. Kerber, P. Rogl, E. Bauer, M. Zehetbauer, J. Alloys Compd. **490**, 19 (2010)
62. J. Yang, G.P. Meisner, C.J. Rawn, H. Wang, B.C. Chakoumakos, J. Martin, G.S. Nolas, P.L. Pedersen, J.K. Stalick, J. Appl. Phys. **102**, 083702 (2007)
63. H. Anno, H. Tashiro, K. Matsubara, in *Proceedings of the Eighteenth International Conference on Thermoelectrics. ICT 1999 Baltimore, Maryland 1999 (Cat. No.99TH8407)* (IEEE, Piscataway, NJ, 1999), p. 169
64. L. Bertini, C. Stiewe, M. Toprak, J. Appl. Phys. **93**(1), 438 (2003)
65. J.P. Fleurial, A. Borshchevsky, T. Caillat, D.T. Morelli, G.P. Meisner, in *Proceedings of the Fifteenth International Conference on Thermoelectrics, Pasadena, California, 1996. (Cat. No.96TH8169)*, vol. 507 (IEEE, New York, NY, 1996), p. 91
66. X. Tang, Q. Zhang, L. Chen, T. Goto, T. Hirai, J. Appl. Phys. **97**(9), 93712 (2005)
67. K.T. Wojciechowski, J. Tobola, J. Leszczynski, J. Compd. **361**, 19 (2003)
68. X.Y. Li, L.D. Chen, J.F. Fan, W.B. Zhang, T. Kawahara, T. Hirai, J. Appl. Phys. **98**, 083702 (2005)

69. J. Y. Jung, M. J. Kim, S. W. You, S. C. Ur, I. H. Kim, in *Proceedings of the Twenty-Fifth International Conference on Thermoelectrics* (ICT, Vienna, Austria, 2006), p. 443
70. S. Liu, B.P. Zhang, J.F. Li, H.L. Zhang, L.D. Zhao, J. Appl. Phys. **102**, 103717 (2007)
71. B. Duan, P. Zhai, P. Wen, S. Zhang, L. Liua, Q. Zhang, Scr. Mater. **67**, 372 (2012)
72. L. Fu, Q. Jiang, J. Yang, J. Peng, Y. Xiao, Y. Luo, Z. Zhou, D. Zhang, J. Mater. Chem. A **4**, 16499 (2016)
73. L. Fu, J. Yang, Q. Jiang, Y. Xiao, Y. Luo, D. Zhang, Z. Zhou, J. Electron. Mater. **45**(3), 1240 (2016)
74. N. Shaheen, X. Shen, M.S. Javed, H. Zhan, L. Guo, R. Alsharafi, T. Huang, X. Lu, G. Wang, X. Zhou, J. Electron. Mater. (2016). https://doi.org/10.1007/s11664-016-5079-z
75. L. Zhang, F. Duan, X. Li, X. Yan, W. Hu, L. Wang, Z. Liu, Y. Tian, B. Xu, J. Appl. Phys. **114**, 083715 (2013)
76. R.C. Mallik, R. Anbalagan, G. Rogl, E. Royanian, P. Heinrich, E. Bauer, P. Rogl, S. Suwas, Acta Mater. **61**, 6698 (2013)
77. K.H. Park, S.C. Ur, I.H. Kim, S.M. Choi, W.S. Seo, J. Korean Phys. Soc. **57**, 1000 (2010)
78. J. Mackey, F. Dynys, B.M. Hudak, B.S. Guiton, A. Sehirlioglu, J. Mater. Sci. **51**, 6117 (2016)
79. X. Su, H. Li, G. Wang, H. Chi, X. Zhou, X. Tang, Q. Zhang, C. Uher, Chem. Mater. **23**, 2948 (2011)
80. W.S. Liu, B.P. Zhang, L.D. Zhao, J.F. Li, Chem. Mater. **20**, 7526 (2008)
81. R.C. Mallik, J.-Y. Jung, S.-C. Ur, I.-H. Kim, Metals Mater. Int. **14**, 615 (2008)
82. J. Navratil, T. Plecha, C. Drasar, V. Kucek, F. Laufek, E. Cernoskova, L. Benes, M. Vlcek, J. Electron. Mater. **45**(6), 2905 (2016)
83. A.U. Khan, K. Kobayashi, D.-M. Tang, Y. Yamauchi, K. Hasegawa, M. Mitome, Y. Xue, B. Jiang, K. Tsuchiya, D. Goldberg, Y. Bando, T. Mori, Nano Energy **31**, 152 (2017)
84. C. Xu, B. Duan, S. Ding, P. Zhai, Q. Zhang, J. Electron. Mater. **43**, 2224 (2014)
85. B. Poudel, Q. Hao, Y. Ma, Y. Lan, A. Minnich, B. Yu, X. Yan, D. Wang, A. Muto, D. Vashaee, X. Chen, J. Liu, M.S. Dresselhaus, G. Chen, Z. Ren, Science **320**, 634 (2008)
86. G.H. Zhu, H. Lee, Y.C. Lan, X.W. Wang, G. Joshi, D.Z. Wang, J. Yang, D. Vashaee, H. Gilbert, A. Pillitteri, M.S. Dresselhaus, G. Chen, Z.F. Ren, Phys. Rev. Lett. **102**(196803) (2009)
87. Y.C. Lan, A.J. Minnich, G. Chen, Z.F. Ren, Adv. Funct. Mater. **20**, 357 (2010)
88. H. Nakagawa, H. Tanaka, A. Kasama, H. Anno, K. Matsubara, in *Proceedings of the Sixteenth International Conference on Thermoelectric* (ICT, Dresden, Germany, 1997), p. 97
89. L. Yang, J.S. Wu, L.T. Zhang, J. Alloys Compd. **375**, 114 (2004)
90. Q. Jie, H. Wang, W. Liu, H. Wang, G. Chen, Z. Ren, Phys. Chem. Chem. Phys. **15**, 6809 (2013)
91. M. Short, F. Bridges, T. Keiber, G. Rogl, P. Rogl, Intermetallics **63**, 80 (2015)
92. L. Zhang, A. Grytsiv, B. Bonarski, M. Kerber, D. Setman, E. Schafler, P. Rogl, E. Bauer, G. Hilscher, M. Zehetbauer, J. Alloys Compd. **494**, 78 (2010)
93. G. Rogl, M. Zehetbauer, M. Kerber, P. Rogl, E. Bauer, Mater. Sci. Forum **1089**, 667–669 (2011)
94. G. Rogl, D. Setman, E. Schafler, J. Horky, M. Kerber, M. Zehetbauer, M. Falmbigl, P. Rogl, E. Royanian, E. Bauer, Acta Mater. **60**, 2146 (2012)
95. G. Rogl, Z. Aabdin, E. Schafler, J. Horky, D. Setman, M. Zehetbauer, M. Kriegisch, O. Eibl, A. Grytsiv, E. Bauer, M. Reinecker, W. Schranz, P. Rogl, J. Alloys Compd. **537**, 183 (2012)
96. G. Rogl, A. Grytsiv, P. Rogl, E. Royanian, E. Bauer, J. Horky, D. Setman, E. Schafler, M. Zehetbauer, Acta Mater. **61**, 6778 (2013)
97. G. Rogl, P. Rogl, in: *Thermoelectric Nanomaterials*, ed. by K. Kuomoto, T. Mori Springer-Verlag, Berlin, Heidelberg, 2013) p.193
98. G. Rogl, A. Grytsiv, P. Rogl, N. Peranio, E. Bauer, M. Zehetbauer, O. Eibl, Acta Mater. **63**, 30 (2014)
99. G. Rogl, A. Grytsiv, J. Horky, R. Anbalagan, E. Bauer, R.C. Mallik, P. Rogl, M. Zehetbauer, Phys. Chem. Chem. Phys. **17**, 3715 (2015)

100. G. Rogl, D. Setman, E. Schafler, J. Horky, M. Kerber, M. Zehetbauer, M. Falmbigl, P. Rogl, E. Bauer, in: *The NATO Science for Peace and Security Programme, Series B: Physics and Biophysics*, ed. by V. Zlatic and A. Hewson, (Springer, Dordrecht, 2012) p. 81
101. R. Anbalagan, G. Rogl, M. Zehetbauer, A. Sharma, P. Rogl, S. Suwas, R.C. Mallik, J. Electron. Mater. **43**(10), 3817 (2014)
102. G. Rogl, P. Rogl, Mater. Today Phys. **3**, 48 (2017)
103. P. Zong, X. Chen, Y. Zhu, Z. Liu, Y. Zeng, L. Chen, J. Mater. Chem. A **3**, 8643 (2015)
104. Q. Zhang, Z. Zhou, M. Dylla, M.T. Agne, Y. Pei, L. Wang, Y. Tang, J. Liao, S. Bai, W. Jiang, L. Chen, G.J. Snyder, Nano Energy **41**, 501 (2017)
105. J. Ding, H. Gu, P. Qiu, X. Chen, Z. Xiong, Q. Zheng, X. Shi, L. Chen, J. Electron. Mater. **42** (3), 382 (2013)
106. J. Ding, R.-H. Liu, H. Gu, L.-D. Chen, J. Inorg. Mater. **29**(2), 209 (2014)
107. X.Y. Zhao, X. Shi, L.D. Chen, W.Q. Zhang, S.Q. Bai, Y.Z. Pei, X.Y. Li, T. Goto, Appl. Phys. Lett. **89**, 092121 (2006)
108. L. Fu, J. Yang, J. Peng, Q. Jiang, Y. Xiao, Y. Luo, D. Zhang, Z. Zhou, M. Zhang, Y. Cheng, F. Cheng, J. Mater. Chem. A **3**(3), 1010 (2015)
109. L. Fu, J. Yang, Y. Xiao, J. Peng, M. Liu, Y. Luo, G. Li, Intermetallics **43**, 79 (2013)
110. X. Zhou, G. Wang, L. Zhang, H. Chi, X. Su, J. Sakamoto, C. Uher, J. Mater. Chem. **22**, 2958 (2012)
111. K. Peng, L. Guo, G. Wang, X. Su, X. Zhou, X. Tang, C. Uher, Sci. Adv. Mater. **9**(3-4), 682 (2017)
112. X. Shi, L.D. Chen, S.Q. Bai, X.Y. Huang, X.Y. Zhao, Q. Yao, J. Appl. Phys. **102**, 103709 (2007)
113. M. Battabyal, B. Priyadarshini, D. Sivaprahasam, N.S. Karthiselva, R. Gopalan, J. Phys. D Appl. Phys. **48**, 455309 (2015)
114. S. Katsuyama, H. Okada, J. Jpn. Soc. Powder Powder Metall. **54**(5), 375 (2007)
115. H.-Y. Zhou, W.-Y. Zhao, W.-T. Zhu, J. Yu, P. Wei, D.-G. Tang, Q.-J. Zhang, J. Electron. Mater. **43**(6), 1498 (2014)
116. S. Wan, X. Huang, P. Qiu, S. Bai, L. Chen, Mater. Des. **67**, 379 (2015)
117. P. Zong, R. Hanus, M. Dylla, Y. Tang, J. Liao, Q. Zhang, G.J. Snyder, L. Chen, Energy Environ. Sci. **10**, 183 (2017)
118. G. Rogl, J. Bursik, A. Grytsiv, S. Puchegger, V. Soprunyuk, W. Schranz, X. Yan, E. Bauer, P. Rogl, Acta Mater. **145**, 359 (2018)
119. B. Feng, J. Xie, G. Cao, T. Zhu, X. Zhao, J. Mater. Chem. A **1**, 13111 (2013)
120. J.L. Mi, X.B. Zhao, T.J. Zhu, J.P. Tu, Appl. Phys. Lett. **91**, 172116 (2007)
121. D. Zhao, M. Zuo, Z. Wang, X. Teng, H. Geng, J. Nanosci. Nanotechnol. **15**(4), 3076 (2015)
122. G. Tan, H. Chi, W. Liu, Y. Zheng, X. Tang, J. He, C. Uher, J. Mater. Chem. C **3**, 8372 (2015)
123. L. Zhou, P. Qiu, C. Uher, X. Shi, L. Chen, Intermetallics **32**, 209 (2013)
124. T. Dahal, Q. Jie, W. Liu, K. Dahal, C. Guo, Y. Lan, Z. Ren, J. Alloys Compd. **623**, 104 (2015)
125. H. Li, X. Tang, Q. Zhang, C. Uher, Appl. Phys. Lett. **94**, 102114 (2009)
126. S. Ballikaya, C. Uher, J. Alloys Compd. **585**, 168 (2014)
127. S. Ballikaya, N. Uzar, S. Yildirim, J.R. Salvador, C. Uher, J. Solid State Chem. **193**, 31 (2012)
128. G. Rogl, A. Grytsiv, K. Yubuta, S. Puchegger, E. Bauer, C. Raju, R.C. Mallik, P. Rogl, Acta Mater. **95**, 201 (2015)
129. B. Duan, J. Yang, J.R. Salvador, Y. He, B. Zhao, S. Wang, P. Wei, F.S. Ohuchi, W. Zhang, R.P. Hermann, O. Gourdon, S.X. Mao, Y. Cheng, C. Wang, J. Liu, P. Zhai, X. Tang, Q. Zhang, J. Yang, Energ. Environ. Sci. **9**, 2090 (2016)
130. S. Wang, J.R. Salvador, J. Yang, P. Wei, B. Duan, J. Yang, NPG Asia Mater. **8**, 285 (2016)
131. M. Matsubara, R. Asahi, J. Electron. Mater. **45**(3), 1669 (2016)
132. L. Zhang, G. Rogl, A. Grytsiv, S. Puchegger, J. Koppensteiner, F. Spieckermann, H. Kabelka, M. Renecker, P. Rogl, M. Zehetbauer, M.A. Carpenter, Mat. Sci. Eng. B **170**, 26 (2010)
133. G. Rogl, S. Puchegger, M. Zehetbauer, A. Grytsiv, in *Proceedings of the Materials Research Society*, 2011, 1325, 845, mrss 11–1325-e03. doi https://doi.org/10.1557/opl.2011.845

134. G. Rogl, P. Rogl, Sc. Adv. Mater. **3**, 1 (2011)
135. P. Wen, H. Mei, P. Zhai, B. Duan, J. Mater. Eng. Perform. **22**, 3561 (2013)
136. P.-A. Zong, L.-D. Chen, J. Inorg. Mater. **32**(1), 33 (2017)
137. P. Wen, P. Zhai, S. Ding, B. Duan, L. Yao, J. Electron. Mater. **46**(5), 2807 (2017)
138. A. Schmitz, C. Schmid, J. de Boor, E. Müller, J. Nanosci. Nanotechnol. **17**, 1547 (2017)
139. M.F. Ashby, *Materials Selection in Mechanical Design*, 3rd edn. (Elsevier, Oxford, 2005)
140. G. Rogl, L. Zhang, P. Rogl, A. Grytsiv, D. Rajs, H. Müller, E. Bauer, J. Koppensteiner, W. Schranz, M. Zehetbauer, J. Appl. Phys. **107**, 043507 (2010)
141. G. Rogl, A. Grytsiv, E. Royanian, P. Heinrich, E. Bauer, P. Rogl, M. Zehetbauer, S. Puchegger, M. Reinecker, W. Schranz, Acta Mater. **61**, 4066 (2013)
142. T. Caillat, J. Sakamoto, L. Lara, A. Jewell, A. Kisor, *Oral Presentation at the Twenty-Third International Conference on Thermoelectrics* (Adelaide, Australia, 2004)
143. D. Zhao, C. Tian, Y. Liu, C. Zhan, L. Chen, J. Alloys Compd. **509**, 3166 (2011)
144. J. Leszczynski, K.T. Wojciechowski, A.L. Malecki, J. Therm. Anal. Calorim. **105**(1), 211 (2011)
145. V. Savchuk, J. Schumann, B. Schupp, G. Behr, N. Mattern, D. Souptel, J. Alloys Compd. **351** (1–2), 248 (2003)
146. K.T. Wojciechowski, J. Leszczynski, R. Gajerski, *Seventh European Workshop on Thermoelectrics*, (Pamplona, Spain, 2002)
147. D. Zhao, C. Tian, S. Tang, Y. Liu, L. Chen, J. Alloys Compd. **504**(2), 552 (2010)
148. K.H. Park, W.S. Seo, S.-M. Choi, I.-H. Kim, J. Korean Phys. Soc. **64**(1), 79 (2014)
149. J.M. Peddle, W. Gaultois, P. Michael, A. Grosvenor, Inorg. Chem. **50**(13), 6263 (2011)
150. J.A. Sigrist, J.D.S. Walker, J.R. Hayes, M.W. Gaultois, A.P. Grosvenor, Solid State Sci. **13** (11), 2041 (2011)
151. X. Xia, P. Qiu, X. Huang, S. Wan, Y. Qiu, X. Li, J. Electron. Mater. **43**(6), 1639 (2014)
152. X. Xia, P. Qiu, X. Shi, X. Li, X. Huang, L. Chen, J. Electron. Mater. **41**(8), 2225 (2012)
153. K.H. Park, S.W. You, S.C. Ur, I.-H. Kim, S.-M. Choi, W.-S. Seo, J. Electron. Mater. **41**(6), 1051 (2012)
154. L.C. Sklad, M.W. Gaultois, A.P. Grosvenor, J. Alloys Compd. **505**(1), 6 (2010)
155. P. Qiu, X. Xia, X. Huang, M. Gu, Y. Qiu, L. Chen, J. Alloys Compd. **612**, 365 (2014)
156. D.K. Shin, I.H. Kim, K.H. Park, S. Lee, W.-S. Seo, Electron. Mater. **44**(6), 1858 (2015)
157. P. Brož, F. Zelenka, Intern. J. Mass Spectronom. **383–384**, 13 (2015)
158. P. Brož, F. Zelenka, Z. Kohoutek, J. Vřešťál, V. Vykoukal, J. Buršík, A. Zemanová, G. Rogl, P. Rogl, Calphad **65**, 1 (2019)
159. N.V. Nong, L.T. Hung, *Oral Presentation at EMN Meeting on Thermoelectric Materials* (Orlando, FL, 2016)
160. N. Pryds, *Oral Presentation at the Autumn School (Thermoelectrics)* (Duisburg, 2015)
161. D.K. Aswal, R. Basu, A. Singh, Energ. Conver. Manage. **114**, 50 (2016)
162. T. Caillat, A. Borshchevsky, J.G. Snyder, in *Proceedings of the AIP Conf. Albuquerque* (New Mexico, 2001), 552, 1107
163. P.H. Ngan, D.V. Christensens, G.J. Snyder, L.T. Hung, S. Linderoth, N.V. Nong, N. Pryds, Phys. Status Solidi A **211**, 9 (2014)
164. J.R. Salvador, J.Y. Cho, Z. Ye, J.E. Moczygemba, A.J. Thompson, J.W. Sharp, J.D. Koenig, R. Maloney, T. Thompson, J. Sakamoto, H. Wang, A.A. Wereszczak, Phys. Chem. Chem. Phys. **16**(24), 12510 (2014)
165. A. Muto, J. Yang, J. Poudel, Z. Ren, Adv. Energy Mater. **3**, 245 (2013)
166. J.Q. Guo, H.Y. Geng, T. Ochi, S. Suzuki, M. Kikuchi, Y. Yamaguchi, S. Ito, J. Electron. Mater. **41**, 1036 (2012)
167. T. Ochi, G. Nie, S. Suzuki, M. Kikuchi, S. Ito, J.Q. Guo, J. Electron. Mater. **43**(6), 2344 (2014)
168. M. Kober, *Oral presentation at EMN Meeting on Thermoelectric Materials* (Orlando, FL, 2016)